



Cite this: *Environ. Sci.: Nano*, 2021, 8, 687

## Natural organic matter surface coverage as a predictor of heteroaggregation between nanoparticles and colloids<sup>†</sup>

Dylan M. Oney and Jeffrey A. Nason \*

Heteroaggregation and eco-corona formation are important, interrelated processes that transform engineered nanoparticles (ENPs) and strongly impact their fate, transport and toxicity in natural and engineered systems. Yet, there is a lack of mechanistic information linking these processes. This work experimentally validates the hypothesis that attachment efficiencies can be predicted on the basis of the fraction of particle surfaces coated by organic matter. Heteroaggregation between branched polyethyleneimine gold nanoparticles (bPEI-AuNPs) and glass beads (a surrogate for naturally occurring suspended particulates) was examined in the presence and absence of Suwannee River natural organic matter (SRNOM) using a recently developed functional assay. Attachment efficiencies for heteroaggregation were quantified in systems where the relative concentrations of ENPs, glass beads and SRNOM were varied so as to systematically control the extent of eco-corona formation on the particle surfaces. Corona formation on the glass microspheres was negligible, but SRNOM readily adsorbed to the bPEI-AuNPs, reducing heteroaggregation. Measured attachment efficiencies were well described by a model correlating attachment efficiencies with the fractional coverage of the bPEI-AuNP surfaces by SRNOM, providing a promising mechanistic link between eco-corona formation and subsequent aggregation behavior. Further, the dependence of attachment efficiencies on the extent of eco-corona formation reveals the necessity that laboratory-based assays control the relative concentrations of ENPs, suspended particulates, and organic matter such that the resultant eco-corona formation is representative of that expected in the relevant environmental system.

Received 5th November 2020,  
Accepted 2nd February 2021

DOI: 10.1039/d0en01094d

rsc.li/es-nano

### Environmental significance

Two key, interrelated processes critical in determining the fate and effects of engineered nanomaterials in aquatic systems are eco-corona formation and heteroaggregation. The affinity of particle surfaces for one another is dictated by the physico-chemical nature of those surfaces and the suspending medium. Although it is well-established that the adsorption of naturally occurring macromolecules to particle surfaces is correlated with heteroaggregation attachment efficiencies, there is a lack of mechanistic information linking these two processes that limits the ability of current fate and transport models to predict environmental behavior. Demonstrating that the fraction of a surface covered with organic matter is predictive of heteroaggregation rates is a first step in filling the present knowledge gap.

### Introduction

When engineered nanoparticles (ENPs) enter natural and engineered systems they are transformed by myriad processes including oxidation/reduction, dissolution, aggregation, and interaction with dissolved organic matter (DOM).<sup>1</sup> These

transformations do not occur in isolation, but often influence one another. For example, macromolecules often accumulate at the surfaces of ENPs suspended in biological and environmental matrices, forming a “corona”.<sup>2,3</sup> This process affects key ENP properties like surface charge, chemical functionality, and reactivity, and influences subsequent transformation via dissolution,<sup>4,5</sup> aggregation,<sup>6–10</sup> and deposition.<sup>11,12</sup>

The aggregation state of ENPs affects particle size and available surface area, key properties controlling ENP reactivity and fate in complex systems. The attachment efficiency,  $\alpha$ , quantifies the probability that two colliding particles will attach and is a critical parameter needed to

School of Chemical, Biological and Environmental Engineering Oregon State University, 116 Johnson Hall, 105 SW 26th St., Corvallis, OR 97331, Oregon.  
E-mail: jeff.nason@oregonstate.edu

† Electronic supplementary information (ESI) available. See DOI: 10.1039/d0en01094d

‡ Current address: US Army Corps of Engineers, Tulsa District, 2488 E 81st St., Tulsa, OK 74137.

predict ENP fate in environmental systems.<sup>13</sup> Although a great deal of early work on ENP fate and transport focused on homoaggregation (aggregation between like particles),<sup>6,14,15</sup> it is widely recognized that heteroaggregation of ENPs with natural colloids is likely to dominate in relevant systems because naturally occurring particles will vastly outnumber ENPs.<sup>16–20</sup> Despite this fact, relatively few studies have examined ENP heteroaggregation processes<sup>16,17,21–29</sup> and even fewer have attempted to quantify attachment efficiencies for heteroaggregation.<sup>30</sup> In the absence of this data, environmental fate and transport models for these materials are forced to rely on assumed values of this key parameter.<sup>19,31,32</sup>

Corona formation is known to affect ENP properties and subsequent homoaggregation.<sup>2</sup> In many cases, corona formation enhances the colloidal stability of ENPs *via* steric and electrostatic forces arising from the adsorbed DOM.<sup>33</sup> However, corona formation can also enhance aggregation in the presence of divalent cations<sup>7,15,34</sup> or when partially coating positively charged ENPs.<sup>35</sup> Properties of engineered coatings<sup>35–37</sup> and DOM<sup>38–40</sup> also influence corona formation and the resultant effects on ENP homoaggregation. In general, these studies lack detailed mechanistic information regarding corona formation and the impacts on  $\alpha$ .<sup>41</sup> As a result, attachment efficiencies are left as empirical fitting factors to account for incomplete theory. The mechanistic aspects of simultaneous corona formation and heteroaggregation have only recently received attention<sup>28,42,43</sup> and have yet to be incorporated into fate and transport models.<sup>44</sup> Due to the outsized role of corona formation on ENP properties and subsequent aggregation behavior, it is imperative that a mechanistic understanding of these interrelated processes be developed.

The processes of heteroaggregation and corona formation result in aggregates with non-uniform surfaces. When the surfaces of colliding particles are heterogeneous, attachment efficiencies are dependent on the nature and extent of that heterogeneity. For example, Healy and La Mer delineated the role of polymer surface coverage on the rates of colloid aggregation *via* bridging flocculation,<sup>45</sup> concepts that have been verified and extended by others.<sup>46–49</sup> Moncho-Jorda *et al.* performed a detailed theoretical analysis of the aggregation of partially coated particles that illustrates the clear dependence of attachment efficiencies on the fractional surface coverage ( $\theta$ ).<sup>50</sup> Similar approaches have been employed in heteroaggregating systems where the “surface coating” occurs *via* attachment of ENPs to the surfaces of natural colloids<sup>17,20,27</sup> or adsorption of DOM to the surface of ENPs.<sup>43</sup> Yet, these concepts have not been extended to three-component systems containing DOM, ENPs and natural colloids.

Wiesner and co-workers have developed a promising functional assay platform to parameterize heteroaggregation.<sup>16,29,51</sup> Briefly, their approach involves suspending ENPs in complex systems containing natural or model colloids and quantifying the rate that ENPs are lost

from suspension *via* heteroaggregation. This approach has been used to determine attachment efficiencies for collisions between various ENPs and activated sludge,<sup>16</sup> algae,<sup>51</sup> soil,<sup>52</sup> and glass beads.<sup>29</sup> Furthermore, measured attachment efficiencies have been correlated with trophic transfer<sup>51</sup> and fate in mesocosms.<sup>53,54</sup> The assay is firmly grounded in colloid theory and has been validated against traditional deposition experiments using packed columns.<sup>29</sup> However, the approach relies on two key assumptions: (1) homoaggregation is negligible and (2) attachment efficiencies are independent of particle concentration.<sup>29</sup> The first assumption can be justified by using an ENP that is stable with respect to homoaggregation and/or by using a model colloid concentration significantly greater than that of the ENPs such that heteroaggregation dominates.<sup>37</sup> Yet, cases where significant homoaggregation occurs have been reported<sup>37,51,52</sup> as has the need to account for homoaggregation in laboratory tests performed at elevated particle concentrations.<sup>30</sup> If valid, the second assumption justifies the use of elevated ENP and colloid concentrations to simplify the assay by speeding the heteroaggregation process and easing the detection of ENPs by techniques like UV-vis spectroscopy. Yet, these attempts to facilitate the operational simplicity may have unintended consequences with respect to technical accuracy, a balance between which these approaches demand.<sup>55–57</sup> While the second assumption is valid for aggregation in the absence of DOM, it is not clear that the same is true for systems where corona formation and concomitant effects on attachment efficiencies become important.

In this work, it was hypothesized that attachment efficiencies for collisions between ENPs and model colloids in the presence of DOM can be predicted on the basis of the fraction of the particle surfaces that are coated by DOM (*i.e.*, surface coverage). This hypothesis was tested using the functional assay developed by Wiesner and co-workers.<sup>29</sup> Rates of attachment between branched-polyethylenimine coated gold nanoparticles (bPEI-AuNPs) and glass beads in the presence of Suwannee River natural organic matter (SRNOM) were measured while varying the relative concentrations of ENPs, glass beads and DOM. These materials were chosen to represent a simple, yet relevant system that would facilitate the systematic examination of DOM surface coverage and heteroaggregation attachment efficiency.  $\text{SiO}_2$  is a prevalent mineral in soil<sup>58</sup> and glass beads have frequently been used as an environmentally relevant collector in particle transport experiments.<sup>33</sup> Independent measurements of DOM adsorption onto the surfaces of the glass beads and the ENPs were made to facilitate the development of a mechanistic link between surface coverage and attachment efficiency. Because the degree of corona formation is likely dictated by the relative concentrations of particles and DOM in a given system, the work also aimed to illustrate the importance of maintaining these ratios at environmentally relevant values in laboratory-based tests used to determine attachment efficiencies.

# Materials and methods

## Materials

Gold nanoparticles coated with 25 kDa branched polyethylenimine (bPEI-AuNP) were purchased from nanoComposix, Inc (NanoXact). The average core diameter reported by the manufacturer was  $61 \pm 8$  nm as measured by transmission electron microscopy. Soda lime glass microspheres were purchased from Cospheric, LLC. The median diameter of the glass beads reported by the manufacturer was  $70 \pm 5$   $\mu\text{m}$  as measured by optical microscopy. Prior to use, glass beads were washed successively in 0.1 M NaOH and 0.1 M HCl (ESI† section 1). Suwanee River natural organic matter (SRNOM) was purchased from the International Humic Substances Society (catalog number 1R101N) and stock solutions were prepared at 15 mg carbon per L as described previously.<sup>35</sup> Sodium chloride (NaCl) (ACS reagent grade, VWR) and HEPES (BioPerformance Certified, Sigma Aldrich) or sodium bicarbonate (NaHCO<sub>3</sub>) (ACS reagent grade, VWR) were used to control ionic strength and pH of solutions, respectively.

## Nanoparticle homoaggregation

The aggregation state of the bPEI-AuNPs in the presence and absence of SRNOM was monitored using time-resolved dynamic light scattering (Brookhaven 90 Plus) and the extent of aggregation ( $D_{\text{h},15}/D_{\text{h},0}$ ) calculated as described previously<sup>35</sup> (Fig. S1†). Additional information on nanoparticle aggregation state was obtained by examining the UV-vis absorbance spectra where shifts of the plasmon resonance peak and shouldering of the spectra at wavelengths larger than the surface plasmon peak are indications of aggregation.<sup>36</sup>

## Electrophoretic mobility

The electrophoretic mobility (EPM) of bPEI-AuNPs in the presence and absence of SRNOM was measured *via* Phase Analysis Light Scattering (Brookhaven ZetaPALS). bPEI-AuNPs (5 mg L<sup>-1</sup>) and SRNOM (0–6 mg C/L) were equilibrated in a solution containing 20 mM NaCl and 1 mM HEPES for 30 minutes prior to measurement (5 measurements of 30 cycles each).

## Quantifying SRNOM adsorption on glass beads

50 mL samples containing SRNOM (0–1.5 mg C/L) and GBs (0 or 60 g L<sup>-1</sup>) in 10 mM sodium bicarbonate and 10 mM sodium chloride (pH = 7  $\pm$  0.2) were combined in 50 mL polyethylene centrifuge tubes and tumbled end-over-end for 24 hours. After equilibration, glass beads were allowed to settle and supernatant solutions were analyzed for total organic carbon, TOC (Shimadzu TOC-VSCH). The difference in organic carbon content between samples with and without glass beads was attributed to SRNOM adsorption. Additionally, adsorption was examined by quartz crystal microbalance with dissipation monitoring (QCMD) by

flowing a solution containing 2 mg C/L of SRNOM in 20 mM sodium chloride and 1 mM HEPES over a soda lime glass sensor and observing the frequency change of the third overtone.

## Quantifying SRNOM adsorption onto bPEI-AuNPs

Quantifying the adsorption of SRNOM onto the bPEI-AuNPs *via* solution depletion was not practical given the cost of the nanoparticles and the high AuNP concentrations needed to reduce solution phase SRNOM concentrations enough to quantify by TOC analysis. As such, changes in the electrophoretic mobility of bPEI-AuNP suspensions following exposure to varying concentrations of SRNOM were used as a surrogate measure of SRNOM adsorption. Data from the electrophoretic mobility experiments described above were used for this analysis. The mobility of bPEI-AuNPs at each SRNOM concentration was subtracted from the mobility of the bPEI-AuNPs in the NaCl/HEPES matrix without SRNOM present. This change in mobility was used to estimate the fraction of the nanoparticle surface covered by SRNOM by fitting to a Langmuir isotherm (further justification in ESI† section 3). The reported TEM diameter of 61 nm was used to calculate nanoparticle surface area.

## Quantifying heteroaggregation

The attachment of bPEI-AuNPs to glass beads was quantified using an adaptation of the suspended particle mixing method developed by Wiesner and co-workers.<sup>16,29</sup> Briefly, 4 mL suspensions containing bPEI-AuNPs and glass beads were combined in 7 mL PFA vessels and mixed at 1000 rpm with a small magnetic stir bar. The estimated shear rate was 23.8 s<sup>-1</sup>.<sup>59</sup> Aliquots of 0.5 mL were taken at prescribed time points and placed in a cuvette where the glass beads (and any attached AuNPs) settled rapidly from suspension. The concentration of the remaining (unheteroaggregated) AuNPs was quantified by UV-vis spectroscopy (Thermo Scientific Orion AquaMate 8000) using a standard curve relating absorbance at the surface plasmon resonance peak (535 nm) to particle concentration (Fig. S3†).

The loss of AuNPs from suspension was fit to a pseudo first order kinetic model of the following form.<sup>16</sup>

$$\ln \frac{N_t}{N_0} = -\alpha \beta B t \quad (1)$$

where  $N_0$  is the nanoparticle number concentration at  $t = 0$ ;  $N_t$  is the nanoparticle number concentration at time  $t$ ,  $\alpha$  is the attachment efficiency,  $\beta$  is the collision frequency between ENPs and glass beads, and  $B$  is the number concentration of glass beads. This model assumes that nanoparticle homoaggregation is negligible, heteroaggregate breakup is negligible at short times, and that heteroaggregation does not significantly reduce the available colloid concentration.<sup>16</sup> For each experiment, the slope of a plot of  $\ln(N_t/N_0)$  vs.  $t$  yielded the pseudo first order rate

constant  $\alpha\beta B$ . Experiments at a given condition were performed in duplicate at a minimum.

All experiments were performed in distilled deionized (DDI) water (Barnstead Nanopure) containing 20 mM NaCl and 1 mM HEPES buffer ( $\text{pH} = 7 \pm 0.2$ ). bPEI-AuNP concentrations were either 2 mg L<sup>-1</sup> or 5 mg L<sup>-1</sup>, glass bead concentrations ranged from 0 to 20 g L<sup>-1</sup>, and SRNOM concentrations ranged from 0 to 2.25 mg C/L. Concentrations of AuNPs and glass beads are both higher than expected in aquatic systems,<sup>60</sup> yet the ratio of the two particle types are environmentally relevant. In the absence of DOM, attachment efficiencies are independent of particle concentration as has been demonstrated previously<sup>29</sup> and confirmed in this work (Fig. 3 and associated discussion). Further, elevated particle concentrations speed the assay and allow the use of UV-vis spectroscopy for AuNP quantification. The ratios of DOM:ENPs and DOM:glass beads were varied systematically to probe the impact of DOM surface coverage on measured attachment efficiencies.

In experiments containing glass beads and SRNOM, the glass beads and SRNOM were equilibrated for 24 hours on a Barnstead|Thermolyne Labquake Rotisserie Shaker before being transferred to the PFA reaction vessels where the AuNPs were subsequently added. A schematic of the experimental protocol and an example calculation showing raw and transformed data can be found in the ESI† (Fig. S4–S7).

## Model development

A conceptual model illustrating the possible interactions between the two particle types in the presence of DOM is presented in Fig. 1. A mathematical formulation of the total attachment efficiency (eqn (2)) illustrates the proposed dependence of the total attachment efficiency on both the individual attachment efficiencies ( $\alpha_{i-j}$ ) between the various possible surfaces and the surface coverage of DOM on the two surfaces ( $\theta_i$ ).<sup>17,20</sup>

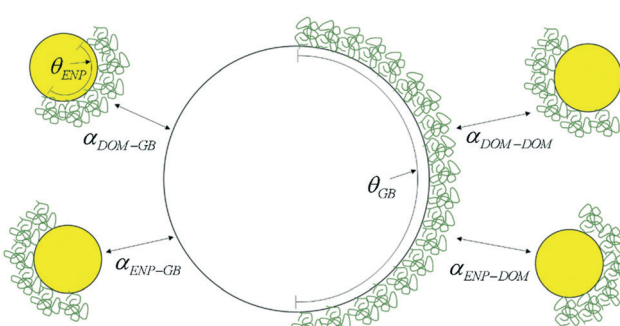


Fig. 1 Conceptual model for collisions between bPEI-AuNPs and glass beads in the presence of SRNOM.  $\alpha_{i-j}$  represent attachment efficiencies between surfaces of type  $i$  and  $j$ .  $\theta_{\text{ENP}}$  and  $\theta_{\text{GB}}$  represent the surface coverage of SRNOM on bPEI-AuNPs and glass beads, respectively.

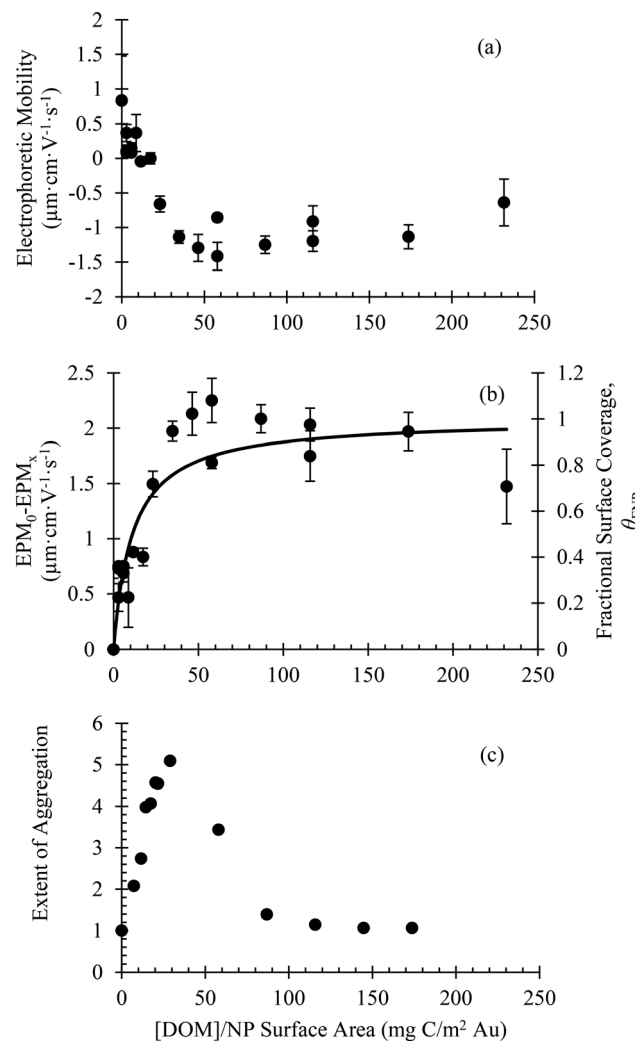
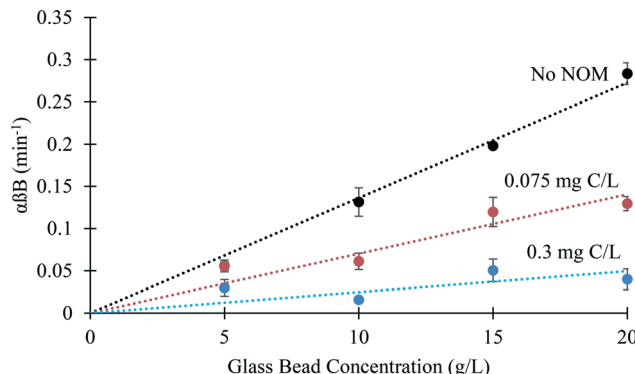


Fig. 2 (a) Electrophoretic mobility of bPEI-AuNPs (5 mg L<sup>-1</sup>); (b) change in electrophoretic mobility and fractional surface coverage ( $\theta_{\text{ENP}}$ ) of bPEI-AuNPs (5 mg L<sup>-1</sup>); and (c) extent of homoaggregation of bPEI-AuNPs (2 mg L<sup>-1</sup>) in the presence of SRNOM. Error bars represent one standard deviation of replicates. Solution conditions included 1 mM HEPES, 20 mM NaCl and varying SRNOM concentrations.

$$\alpha_{\text{hetero}}^{\text{tot}} = (1 - \theta_{\text{ENP}})(1 - \theta_{\text{GB}})\alpha_{\text{ENP-GB}} + (1 - \theta_{\text{ENP}})\theta_{\text{GB}}\alpha_{\text{ENP-DOM}} + \theta_{\text{ENP}}(1 - \theta_{\text{GB}})\alpha_{\text{DOM-GB}} + \theta_{\text{ENP}}\theta_{\text{GB}}\alpha_{\text{DOM-DOM}} \quad (2)$$

In eqn (2),  $\alpha_{\text{hetero}}^{\text{tot}}$  is the total heteroaggregation attachment efficiency between partially coated surfaces;  $\alpha_{\text{ENP-GB}}$  is the attachment efficiency between the glass bead surface and the surface of the engineered nanoparticles;  $\alpha_{\text{ENP-DOM}}$  is the attachment efficiency between the surface of the engineered nanoparticles and DOM adsorbed on the glass bead surface;  $\alpha_{\text{DOM-GB}}$  is the attachment efficiency between DOM adsorbed on the engineered nanoparticle surface and the glass bead surface;  $\alpha_{\text{DOM-DOM}}$  is the attachment efficiency between DOM adsorbed on the nanoparticle surface and DOM adsorbed on the glass bead surface; and  $\theta_{\text{ENP}}$  and  $\theta_{\text{GB}}$  represent the fractional coverage of DOM on the surface of ENPs and glass



**Fig. 3** Influence of GB concentration,  $B$ , and SRNOM concentration on the pseudo first order rate constant,  $\alpha\beta B$ . Error bars represent standard deviation of replicates. Linear trendlines fit through the origin are shown as eye-guides.

beads, respectively. When no DOM is present,  $\alpha_{\text{hetero}}^{\text{tot}}$  is equal to  $\alpha_{\text{ENP-GB}}$ .  $\alpha$  and  $\theta$  can theoretically vary between 0 and 1.

## Results and discussion

### bPEI-AuNP characteristics and behavior in the presence of SRNOM

The electrophoretic mobility of bPEI-AuNPs in the presence of varying concentrations of SRNOM is presented in Fig. 2a. In the absence of SRNOM, the bPEI-AuNPs were positively charged. As the DOM:ENP ratio increased, the electrophoretic mobility became less positive, ultimately reversing and becoming negative. This change in electrophoretic mobility is indicative of SRNOM adsorption to the bPEI-AuNPs. The magnitude of the change in electrophoretic mobility with increasing DOM:ENP ratio and the estimated relative fractional surface coverage of SRNOM on the bPEI-AuNPs ( $\theta_{\text{ENP}}$ ) are shown in Fig. 2b (see section 3 of the ESI† for details).

The adsorption of SRNOM to the bPEI-AuNPs induced homoaggregation (Fig. 2c). The extent of aggregation increased with increasing DOM:ENP ratio, reaching a maximum at approximately 30 mg C/m<sup>2</sup> Au. Further increases in DOM concentration resulted in decreased homoaggregation. Only slight size changes were observed at DOM:NP ratios greater than 120 mg C/m<sup>2</sup> Au where surface coverage was nearly complete ( $\theta_{\text{ENP}} \approx 1.0$ ). These results are consistent with previous findings and explained by DOM facilitated interparticle bridging *via* an electrostatic patch mechanism.<sup>35</sup> Agreement of these results with previous work using 12 nm bPEI AuNPs when compared on the basis of DOM:ENP surface area (Fig. S8†) further confirms that DOM surface coverage controls the stability of bPEI-AuNPs with respect to homoaggregation.

### SRNOM adsorption to glass beads

Negligible adsorption of SRNOM onto glass beads was observed by solution depletion (Fig. S9†) and quartz crystal microbalance using soda-lime glass coated sensors (Fig.

S10†). There are conflicting reports in the literature of NOM adsorption onto silica surfaces. Franchi and O'Melia reported adsorption of Suwanee River humic acid (SRHA) to soda-lime glass beads,<sup>61</sup> but Yang *et al.*<sup>62</sup> found no adsorption of SRHA to silica nanoparticles and Li *et al.*<sup>63</sup> reported negligible adsorption of Suwanee River humic and fulvic acid onto SiO<sub>2</sub> surfaces by quartz crystal microbalance over a range of pH values. At the conditions of this work (pH = 7 and relatively low ionic strength), both the SRNOM and the soda-lime glass bead surfaces are negatively charged. It is expected that electrostatic repulsion between SRNOM and the soda-lime glass surfaces explain the observed lack of adsorption in this work.

### Heteroaggregation of bPEI AuNPs with glass beads in the absence of SRNOM

In the absence of SRNOM, bPEI AuNPs rapidly attached to the glass beads and were subsequently removed from suspension following settling. SEM images confirm attachment of the bPEI-AuNPs to the glass beads (Fig. S11†). Consistent with theory, and as has been demonstrated previously,<sup>29</sup> the rate constant for heteroaggregation ( $\alpha\beta B$ ) is proportional to the glass bead concentration ( $B$ ) (Fig. 3). Results and analysis from an example experiment are shown in Fig. S5–S7.†

### Heteroaggregation of bPEI AuNPs with glass beads in the presence of SRNOM

Attachment efficiencies for collisions between bPEI AuNPs and glass beads decreased in the presence of SRNOM as evidenced by reduced slopes in the trends of  $\alpha\beta B$  vs.  $B$  with increasing SRNOM concentration (Fig. 3). These results are consistent with those of Turner *et al.*<sup>52</sup> who observed a decrease in the attachment of bPEI AuNPs to a model soil when organic matter was present. According to the conceptual model outlined in Fig. 1, this reduction could be the result of SRNOM adsorption onto the bPEI AuNPs, the glass beads, or both. However, SRNOM adsorption onto the glass beads is negligible, a fact further confirmed by the linearity of the trend in  $\alpha\beta B$  vs.  $B$  in the presence of SRNOM. If SRNOM were adsorbing onto the surfaces of the glass beads, it is expected that surface coverage ( $\theta_{\text{GB}}$ ) would vary as function of the SRNOM to glass bead ratio, resulting in convex curvature in the  $\alpha\beta B$  vs.  $B$  trend. The dependence of attachment efficiencies in the presence of organic matter on the relative surface area of nanoparticle and glass bead surfaces was recognized by Geitner *et al.*<sup>29</sup> in their work with PVP-coated silver nanoparticles and glass beads. In that work, adsorption of humic acid to the nanoparticle surfaces was hypothesized to be the more important process in suspended particle mixing experiments like those performed here.

**Impact of homoaggregation on measured values of  $\alpha\beta B$ .** As demonstrated above, bPEI AuNPs homoaggregate in the presence of SRNOM when the ratio of the two components is less than approximately 120 mg C/m<sup>2</sup> Au. This reduction in

the number of primary ENPs and formation of bPEI-AuNP homoaggregates has the potential to interfere with the measurement of  $\alpha\beta B$  in batch heteroaggregation tests in the following ways: (1) homoaggregation alters the UV-vis spectra used to quantify free ENP concentration resulting in a loss of absorbance at the surface plasmon resonance peak and the formation of a secondary peak at higher wavelengths;<sup>36</sup> (2)  $\beta$  is a function of particle size and may vary as homoaggregation proceeds; and (3) ENP homoaggregates may be removed from suspension during the settling step.

With respect to the first concern, bPEI-AuNP homoaggregation was rapid and apparent in the first ( $t \approx 0$ ) samples collected in tests without glass beads (Fig. S12†). Subsequent samples did not indicate continued homoaggregation, only loss of absorbance across all wavelengths (Fig. S13†). Because  $\alpha\beta B$  is calculated on the basis of  $N/N_0$  (eqn (1)), the fact that  $t \approx 0$  samples were already aggregated and didn't continue to aggregate during the heteroaggregation tests indicates that homoaggregation didn't impact heteroaggregation results. With respect to the second concern, estimated collision efficiencies between 60 nm bPEI-AuNPs and 70  $\mu\text{m}$  glass beads were <1% different from those for the largest ( $\sim 300$  nm) homoaggregates (ESI† section 10). Finally, the settling velocities of the largest measured homoaggregates were not sufficient to result in the loss of bPEI-AuNP homoaggregates prior to measurement (ESI† section 10). In summary, the homoaggregation of bPEI-AuNPs induced by SRNOM did not impact the results of the heteroaggregation batch tests reported here. Turner *et al.*<sup>52</sup> reached a similar conclusion with regard to the impact of homoaggregation on the quantification of  $\alpha\beta B$  for heteroaggregation between citrate stabilized AuNPs and a model soil. As in that system, plots of  $\alpha\beta B$  vs.  $B$  in this work are linear (Fig. 3), a further indication that heteroaggregation is dominant in the experiments reported here.

**Impact of DOM:ENP ratio.** To better isolate the effect of SRNOM on heteroaggregation attachment efficiencies, experiments at a single glass bead concentration ( $20 \text{ g L}^{-1}$ ) are examined in greater detail. The influence of the DOM:

ENP ratio was evaluated by comparing values of  $\alpha\beta B$  measured at two ENP concentrations ( $2$  and  $5 \text{ mg L}^{-1}$ ) and varying SRNOM concentration. At both ENP concentrations, the rate of heteroaggregation decreases with increasing SRNOM concentration (Fig. 4). This reduced rate of attachment is attributed to increases in  $\theta_{\text{ENP}}$  as the ENP surfaces are increasingly coated by SRNOM (Fig. 2b). The fact that data for the two ENP concentrations overlap when normalized by ENP surface area indicates that this is a surface coverage dependent process. Stated another way, this demonstrates that changing the ENP concentration while keeping the DOM concentration constant results in different measured attachment efficiencies. This can be clearly seen when the same data are plotted as a function of SRNOM concentration without accounting for ENP surface area (Fig. S14†).

**ENP losses to vessel walls.** In control experiments without SRNOM and glass beads there was a measurable loss of ENPs from solution (Fig. S15†). This loss is attributed to the bPEI-AuNPs attaching to the vessel walls. The extent of this loss decreased with increasing SRNOM concentration in a manner analogous to that observed in the presence of glass beads (Fig. S16†). As the bPEI-AuNPs became increasingly coated with SRNOM, the attachment efficiency between the ENPs and the vessel walls decreased. These losses were accounted for in the model as described below.

### Modeling

The conceptual model developed in eqn (2) is now applied to the experimental data collected above. On the basis of the adsorption experiments with SRNOM and glass beads it can be assumed that the surface coverage of SRNOM on the glass bead surfaces is zero ( $\theta_{\text{GB}} \approx 0$ ) and that the attachment efficiency between SRNOM coated surfaces and bare glass bead surfaces is also zero ( $\alpha_{\text{NOM-GB}} \approx 0$ ). Furthermore, because no aggregation of SRNOM was observed at the conditions of these tests, it can also be assumed that the attachment efficiency between two SRNOM coated surfaces is

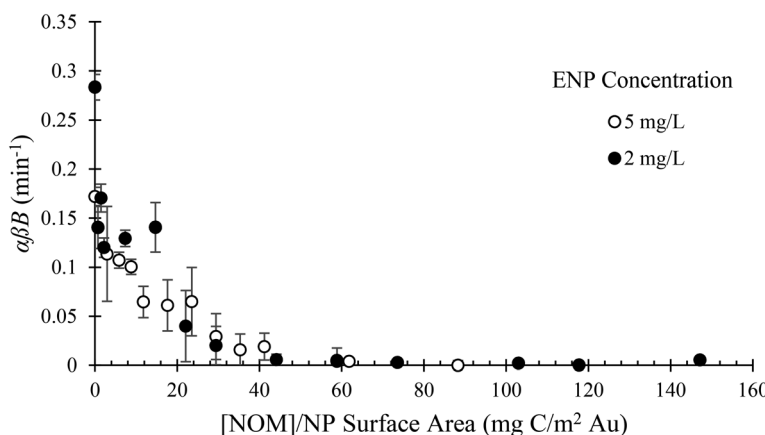


**Fig. 4** Pseudo-first order rate constants ( $\alpha\beta B$ ) for attachment of bPEI-AuNPs ( $2 \text{ mg L}^{-1}$  or  $5 \text{ mg L}^{-1}$ ) to glass beads ( $20 \text{ g L}^{-1}$ ) in  $1 \text{ mM}$  HEPES,  $20 \text{ mM}$  NaCl, and varying concentrations of SRNOM. Error bars represent one standard deviation of replicates.

also zero ( $\alpha_{\text{NOM-NOM}} \approx 0$ ). As such, the conceptual model in eqn (2) simplifies to eqn (3), where the total attachment efficiency for heteroaggregation is only a function of the attachment efficiency between the bare bPEI-AuNPs and the bare glass beads and the fraction of the bPEI-AuNP surfaces coated by SRNOM.

$$\alpha_{\text{hetero}}^{\text{tot}} = (1 - \theta_{\text{ENP}})\alpha_{\text{ENP-GB}} \quad (3)$$

The loss of bPEI-AuNPs to the vessel walls was incorporated into the model using a second term with the same form as eqn (3). Because the product  $\alpha\beta B$  is measured in these tests, the model expression is rewritten to include the additional loss term as follows:

$$(\alpha\beta B)_{\text{model}} = (1 - \theta_{\text{ENP}})[\alpha_{\text{ENP-GB}}\beta B + \alpha_{\text{ENP-wall}}k_{\text{wall}}] \quad (4)$$

where  $\alpha_{\text{ENP-wall}}$  is the attachment efficiency between the bare bPEI surfaces and the vessel walls and  $k_{\text{wall}}$  represents the effective first-order collision frequency between nanoparticles and the vessel walls. The term in square brackets represents the pseudo first order rate constant for the loss of bPEI-AuNPs in the absence of SRNOM and was quantified as the average measured at bPEI-AuNP concentrations of 2 and 5 mg L<sup>-1</sup>.

Using only the average value of the pseudo-first order rate constant for the loss of bPEI-AuNPs from suspension in the absence of SRNOM and the relationship between surface coverage and the DOM:ENP ratio (Fig. 2b), the predicted rate constant was calculated as a function of DOM:ENP ratio using eqn (4) and is plotted alongside the experimental data in Fig. 5. Fig. S17† presents this same data as a function of  $\theta_{\text{ENP}}$ . The model clearly captures the trend in the data, further confirming the dependence of the process on surface coverage. However, the model overpredicts attachment rate constants for a broad range of DOM:ENP ratios. It is hypothesized that this overprediction results from incomplete accounting of geometric considerations

stemming from the random sequential adsorption of SRNOM molecules onto the bPEI AuNP surfaces, and the relative sizes of the SRNOM, bPEI AuNPs and glass beads.<sup>64</sup>

As shown in the inset to Fig. 5, attachment can be prevented at conditions where  $\theta_{\text{ENP}} < 1$  due to blocking by previously adsorbed molecules. In addition to physical blocking, unfavorable electrostatic and steric interactions between NOM molecules likely further reduce the effective available surface area for attachment between the coated AuNPs and the glass bead surface. Blocking functions have been derived for various adsorption scenarios using random sequential adsorption (RSA) theory.<sup>64</sup> However, the authors are not aware of theoretical functions for the present problem of partially coated particles attaching to a collector. In the absence of explicit information regarding the size and polydispersity of adsorbed SRNOM macromolecules, a blocking function of the following form is proposed to replace the quantity  $(1 - \theta_{\text{ENP}})$  in eqn (4):

$$\phi = \begin{cases} \left(1 - \frac{\theta_{\text{ENP}}}{\theta_{\text{limit}}}\right) & \theta_{\text{ENP}} \leq \theta_{\text{limit}} \\ 0 & \theta_{\text{ENP}} > \theta_{\text{limit}} \end{cases} \quad (5)$$

where  $\theta_{\text{limit}}$  represents the fractional surface coverage of SRNOM on the bPEI-AuNP surface beyond which attachment to the glass beads is prevented. The form of the proposed blocking function is consistent with the formulation for adsorption of spherical particles onto a spherical collector<sup>65</sup> and for adsorption of larger particles onto a surface pre-coated with smaller particles.<sup>66</sup> Further, consistent with both of these cases,  $\theta_{\text{limit}}$  is expected to be dependent on the ratio of the SRNOM and bPEI particle radii. In this work, SRNOM is a heterogeneous mix of macromolecules that are varied in size and not necessarily well-represented as hard spheres. As a result,  $\theta_{\text{limit}}$  cannot easily be estimated from first principles. As shown in Fig. 5, implementing the modified blocking function with  $\theta_{\text{limit}}$  as the sole fitting parameter ( $\theta_{\text{limit}} = 0.83$ ) provides a substantially improved fit to the experimental data.

In sum, these experimental results confirm the theoretical dependence of the heteroaggregation attachment efficiency on surface coverage<sup>27,43,50</sup> and, through the proposed model, provide an explicit link between corona formation and attachment efficiency. The present work is limited in that DOM did not adsorb to a significant extent on the glass bead surfaces. As a result, the conceptual model was greatly simplified. Future research with a model colloid that also adsorbs DOM is necessary to validate these findings for cases where surface coverage on both the nanoparticle and colloid surfaces vary. Nonetheless, the clear dependence of heteroaggregation rate on the extent to which an eco-corona formed on the ENP surfaces indicates that the basis for this conceptual model is valid. Additional work is also necessary to further refine the geometric blocking functions so as to accurately represent collisions between surfaces partially coated with DOM on the basis of DOM, ENP and colloid properties.

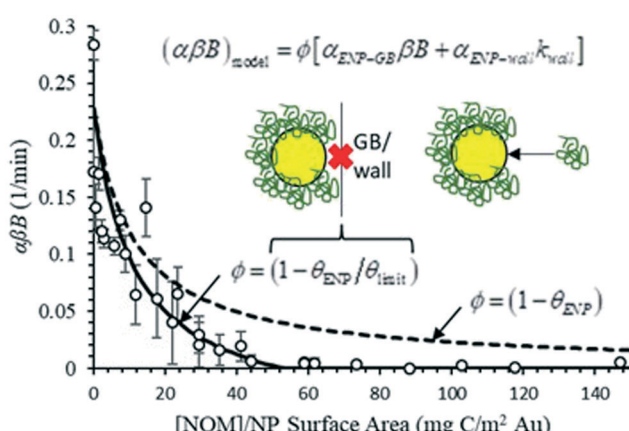


Fig. 5 Experimentally measured pseudo first-order heteroaggregation rate constants ( $\alpha\beta B$ ) for collisions between bPEI AuNPs and glass beads and comparison with model predictions.

## Conclusions

It is well established that eco-corona formation impacts collision efficiencies between particles in the environment. Yet, existing fate and transport models do not explicitly account for the process of eco-corona formation, nor the subsequent effects of these transformations on aggregation processes. The present work takes an important step in this direction, offering organic matter surface coverage as a mechanistic link between eco-corona formation and resulting attachment efficiencies. With the proposed framework, quantification of DOM adsorption onto particle surfaces, paired with knowledge of affinities between relevant surfaces (bare and DOM coated particles) can be used to predict attachment efficiencies in complex systems containing ENPs, DOM and natural colloids.

The extent of corona formation on a given surface will be dictated by the relative concentrations of DOM and available surface area for adsorption, the character of the DOM and the particle surfaces, and the aqueous chemistry. This work strengthens previous assertions that laboratory experiments designed to quantify attachment efficiencies must take care to ensure that the DOM:ENP ratios utilized in these experiments are representative of those expected in the environment.<sup>35,37</sup> DOM:ENP ratios in natural and engineered systems are expected to be quite high (>1000 mass C/mass NP).<sup>60,67,68</sup> If ENP concentrations are elevated in laboratory tests, this must be done in such a way that the extent of the resulting eco-corona formation ( $\theta_{ENP}$ ) remains relevant to the system under investigation. This requires knowledge of how  $\theta_{ENP}$  varies with DOM:ENP ratio (*i.e.*, an adsorption isotherm).

This principle also extends to ensuring representative eco-corona formation on natural colloids or surrogates used in assays designed to determine heteroaggregation attachment efficiencies. Here, environmentally relevant DOM:NC ratios (and resulting values of  $\theta_{NC}$ ) must be maintained. For example, in their work applying glass beads as a surrogate natural colloid for estimation of heteroaggregation attachment efficiencies in wetland mesocosms, Geitner *et al.*<sup>53</sup> aged glass beads in mesocosm water prior to use as a way of achieving representative eco-corona formation. Similar approaches are suggested in future work using surrogates for naturally occurring colloids.

Finally, care must be taken to ensure that the relative concentrations of ENPs and natural colloids are chosen such that heteroaggregation dominates in assays designed to determine heteroaggregation attachment efficiencies. Regardless of study design, appropriate control experiments are needed to verify that homoaggregation does not occur to a significant extent, or as was the case in this work and that of Turner *et al.*,<sup>52</sup> that homoaggregation doesn't impact the results of the surface affinity functional assay.

The current study is limited in focusing on a single, positively charged nanoparticle, a single model colloid that did not adsorb DOM, and a single DOM surrogate. Natural

aquatic systems are expected to contain a diverse population of suspended particulates that are heterogeneous with respect to particle size and surface chemistry and DOM of widely varying character. However, this simplified model system was purposely chosen to facilitate the development of mechanistic understanding. The concentrations of AuNPs and glass beads were not environmentally relevant, but their relative concentrations were. Further, by systematically varying the ratio of DOM:ENPs, the dependence of heteroaggregation on surface coverage was revealed. The results of this study can be translated to the conditions expected in the environment by focusing on the ratio of the three relevant species and the resulting surface coverage. Thus, it is predicted that bPEI-AuNPs would be completely coated by SRNOM at environmentally relevant DOM:ENP ratios, resulting in negligible homo- and heteroaggregation in natural systems.

Demonstration of the relationship between DOM surface coverage and resulting attachment efficiencies provides a needed mechanistic link between the processes of eco-corona formation and ENP aggregation. Yet, further work is necessary to extend the model developed here to more complex systems involving a broader array of ENP types, DOM, and colloid surrogates or naturally occurring particles. Detailed investigations of the rate and extent of DOM adsorption onto engineered and natural particle surfaces are necessary, as are efforts to quantify the individual affinities between bare and DOM coated particle surfaces ( $\alpha_{i-j}$ ) that appropriately accounts for random sequential adsorption theory and geometric blocking between heterogeneously coated surfaces. Identification of DOM and ENP properties that are predictive of DOM adsorption are also needed. Efforts in these areas are expected to yield the parameters necessary to predict attachment efficiencies for relevant environmental aquatic systems.

## Author contributions

Conceptualization: JAN; funding acquisition, JAN; investigation, DMO and JAN; methodology, DMO and JAN; project administration, JAN; supervision, JAN; writing – original draft, DMO; writing – review and editing, DMO and JAN.

## Conflicts of interest

There are no conflicts of interest to declare.

## Acknowledgements

This research was supported by the National Science Foundation (NSF) Grant No. 1255020. Any opinions, findings, and conclusions or recommendations expressed in this material are those of the author(s) and do not necessarily reflect the views of the NSF. Special thanks to K. Motter (Institute for Water and Watersheds Collaboratory) for assistance with TOC/DOC measurements.

## References

- 1 G. V. Lowry, K. B. Gregory, S. C. Apte and J. R. Lead, Transformations of Nanomaterials in the Environment, *Environ. Sci. Technol.*, 2012, **46**(13), 6893–6899.
- 2 S. M. Louie, R. D. Tilton and G. V. Lowry, Critical review: impacts of macromolecular coatings on critical physicochemical processes controlling environmental fate of nanomaterials, *Environ. Sci.: Nano*, 2016, **3**(2), 283–310.
- 3 T. Cedervall, I. Lynch, S. Lindman, T. Berggard, E. Thulin, H. Nilsson, K. A. Dawson and S. Linse, Understanding the nanoparticle-protein corona using methods to quantify exchange rates and affinities of proteins for nanoparticles, *Proc. Natl. Acad. Sci. U. S. A.*, 2007, **104**(7), 2050–2055.
- 4 J. Liu and R. H. Hurt, Ion release kinetics and particle persistence in aqueous nano-silver colloids, *Environ. Sci. Technol.*, 2010, **44**(6), 2169–2175.
- 5 S. W. Bian, I. A. Mudunkotuwa, T. Rupasinghe and V. H. Grassian, Aggregation and Dissolution of 4 nm ZnO Nanoparticles in Aqueous Environments: Influence of pH, Ionic Strength, Size, and Adsorption of Humic Acid, *Langmuir*, 2011, **27**(10), 6059–6068.
- 6 S. E. Mylon, K. L. Chen and M. Elimelech, Influence of natural organic matter and ionic composition on the kinetics and structure of hematite colloid aggregation: Implications to iron depletion in estuaries, *Langmuir*, 2004, **20**(21), 9000–9006.
- 7 K. L. Chen, S. E. Mylon and M. Elimelech, Aggregation kinetics of alginate-coated hematite nanoparticles in monovalent and divalent electrolytes, *Environ. Sci. Technol.*, 2006, **40**(5), 1516–1523.
- 8 K. L. Chen and M. Elimelech, Influence of humic acid on the aggregation kinetics of fullerene (C-60) nanoparticles in monovalent and divalent electrolyte solutions, *J. Colloid Interface Sci.*, 2007, **309**(1), 126–134.
- 9 Y. Zhang, Y. S. Chen, P. Westerhoff, K. Hristovski and J. C. Crittenden, Stability of commercial metal oxide nanoparticles in water, *Water Res.*, 2008, **42**(8–9), 2204–2212.
- 10 R. F. Domingos, N. Tufenkji and K. J. Wilkinson, Aggregation of Titanium Dioxide Nanoparticles: Role of a Fulvic Acid, *Environ. Sci. Technol.*, 2009, **43**(5), 1282–1286.
- 11 T. Ben-Moshe, I. Dror and B. Berkowitz, Transport of metal oxide nanoparticles in saturated porous media, *Chemosphere*, 2010, **81**(3), 387–393.
- 12 A. J. Pelley and N. Tufenkji, Effect of particle size and natural organic matter on the migration of nano- and microscale latex particles in saturated porous media, *J. Colloid Interface Sci.*, 2008, **321**(1), 74–83.
- 13 A. Praetorius, N. Tufenkji, K. U. Goss, M. Scheringer, F. von der Kammer and M. Elimelech, The road to nowhere: equilibrium partition coefficients for nanoparticles, *Environ. Sci.: Nano*, 2014, **1**(4), 317–323.
- 14 K. L. Chen and M. Elimelech, Aggregation and deposition kinetics of fullerene (C-60) nanoparticles, *Langmuir*, 2006, **22**(26), 10994–11001.
- 15 D. P. Stankus, S. E. Lohse, J. E. Hutchison and J. A. Nason, Interactions between natural organic matter and gold nanoparticles stabilized with different organic capping agents, *Environ. Sci. Technol.*, 2011, **45**(8), 3238–3244.
- 16 L. E. Barton, M. Therezien, M. Auffan, J. Y. Bottero and M. R. Wiesner, Theory and Methodology for Determining Nanoparticle Affinity for Heteroaggregation in Environmental Matrices Using Batch Measurements, *Environ. Eng. Sci.*, 2014, **31**(7), 421–427.
- 17 A. Praetorius, J. Labille, M. Scheringer, A. Thill, K. Hungerbuhler and J. Y. Bottero, Heteroaggregation of Titanium Dioxide Nanoparticles with Model Natural Colloids under Environmentally Relevant Conditions, *Environ. Sci. Technol.*, 2014, **48**(18), 10690–10698.
- 18 J. T. Quik, M. C. Stuart, M. Wouterse, W. Peijnenburg, A. J. Hendriks and D. van de Meent, Natural colloids are the dominant factor in the sedimentation of nanoparticles, *Environ. Toxicol. Chem.*, 2012, **31**(5), 1019–1022.
- 19 A. L. Dale, G. V. Lowry and E. A. Casman, Stream Dynamics and Chemical Transformations Control the Environmental Fate of Silver and Zinc Oxide Nanoparticles in a Watershed-Scale Model, *Environ. Sci. Technol.*, 2015, **49**(12), 7285–7293.
- 20 M. Therezien, A. Thill and M. R. Wiesner, Importance of heterogeneous aggregation for NP fate in natural and engineered systems, *Sci. Total Environ.*, 2014, **485**, 309–318.
- 21 J. B. Liu, Y. S. Hwang and J. J. Lenhart, Heteroaggregation of bare silver nanoparticles with clay minerals, *Environ. Sci.: Nano*, 2015, **2**(5), 528–540.
- 22 J. Labille, C. Harns, J. Y. Bottero and J. Brant, Heteroaggregation of Titanium Dioxide Nanoparticles with Natural Clay Colloids, *Environ. Sci. Technol.*, 2015, **49**(11), 6608–6616.
- 23 P. D. Yates, G. V. Franks, S. Biggs and G. J. Jameson, Heteroaggregation with nanoparticles: effect of particle size ratio on optimum particle dose, *Colloids Surf. A*, 2005, **255**(1–3), 85–90.
- 24 K. A. Huynh, J. M. McCaffery and K. L. Chen, Heteroaggregation of Multiwalled Carbon Nanotubes and Hematite Nanoparticles: Rates and Mechanisms, *Environ. Sci. Technol.*, 2012, **46**(11), 5912–5920.
- 25 A. R. M. N. Afroz, I. A. Khan, S. M. Hussain and N. B. Saleh, Mechanistic Heteroaggregation of Gold Nanoparticles in a Wide Range of Solution Chemistry, *Environ. Sci. Technol.*, 2013, **47**(4), 1853–1860.
- 26 J. T. K. Quik, I. Velzeboer, M. Wouterse, A. A. Koelmans and D. van de Meent, Heteroaggregation and sedimentation rates for nanomaterials in natural waters, *Water Res.*, 2014, **48**, 269–279.
- 27 B. M. Smith, D. J. Pike, M. O. Kelly and J. A. Nason, Quantification of Heteroaggregation between Citrate-Stabilized Gold Nanoparticles and Hematite Colloids, *Environ. Sci. Technol.*, 2015, **49**(21), 12789–12797.
- 28 O. Oriekhova and S. Stoll, Heteroaggregation of CeO<sub>2</sub> nanoparticles in presence of alginate and iron (III) oxide, *Sci. Total Environ.*, 2019, **648**, 1171–1178.

29 N. K. Geitner, N. J. O'Brien, A. A. Turner, E. J. Cummins and M. R. Wiesner, Measuring Nanoparticle Attachment Efficiency in Complex Systems, *Environ. Sci. Technol.*, 2017, **51**(22), 13288–13294.

30 A. Praetorius, E. Badetti, A. Brunelli, A. Clavier, J. A. Gallego-Urrea, A. Gondikas, M. Hassellöv, T. Hofmann, A. Mackevica, A. Marcomini, W. Peijnenburg, J. T. K. Quik, M. Seijo, S. Stoll, N. Tepe, H. Walch and F. von der Kammer, Strategies for determining heteroaggregation attachment efficiencies of engineered nanoparticles in aquatic environments, *Environ. Sci.: Nano*, 2020, **7**(2), 351–367.

31 A. Praetorius, M. Scheringer and K. Hungerbühler, Development of Environmental Fate Models for Engineered Nanoparticles—A Case Study of TiO<sub>2</sub> Nanoparticles in the Rhine River, *Environ. Sci. Technol.*, 2012, **46**(12), 6705–6713.

32 N. Sani-Kast, M. Scheringer, D. Slomberg, J. Labille, A. Praetorius, P. Ollivier and K. Hungerbuhler, Addressing the complexity of water chemistry in environmental fate modeling for engineered nanoparticles, *Sci. Total Environ.*, 2015, **535**, 150–159.

33 A. R. Petosa, D. P. Jaisi, I. R. Quevedo, M. Elimelech and N. Tufenkji, Aggregation and deposition of engineered nanomaterials in aquatic environments: role of physicochemical interactions, *Environ. Sci. Technol.*, 2010, **44**(17), 6532–6549.

34 K. L. Chen, S. E. Mylon and M. Elimelech, Enhanced aggregation of alginate-coated iron oxide (hematite) nanoparticles in the presence of calcium, strontium, and barium cations, *Langmuir*, 2007, **23**(11), 5920–5928.

35 M. C. Surette and J. A. Nason, Effects of surface coating character and interactions with natural organic matter on the colloidal stability of gold nanoparticles, *Environ. Sci.: Nano*, 2016, **3**(5), 1144–1152.

36 M. C. Surette, J. A. Nason and R. Kaegi, The influence of surface coating functionality on the aging of nanoparticles in wastewater, *Environ. Sci.: Nano*, 2019, **6**(8), 2470–2483.

37 M. C. Surette and J. A. Nason, Nanoparticle aggregation in a freshwater river: the role of engineered surface coatings, *Environ. Sci.: Nano*, 2019, **6**(2), 540–553.

38 J. A. Nason, S. A. McDowell and T. W. Callahan, Effects of natural organic matter type and concentration on the aggregation of citrate-stabilized gold nanoparticles, *J. Environ. Monit.*, 2012, **14**(7), 1885–1892.

39 S. M. Louie, R. D. Tilton and G. V. Lowry, Effects of Molecular Weight Distribution and Chemical Properties of Natural Organic Matter on Gold Nanoparticle Aggregation, *Environ. Sci. Technol.*, 2013, **47**(9), 4245–4254.

40 S. M. Louie, E. R. Spielman-Sun, M. J. Small, R. D. Tilton and G. V. Lowry, Correlation of the Physicochemical Properties of Natural Organic Matter Samples from Different Sources to Their Effects on Gold Nanoparticle Aggregation in Monovalent Electrolyte, *Environ. Sci. Technol.*, 2015, **49**(4), 2188–2198.

41 A. Philippe and G. E. Schaumann, Interactions of Dissolved Organic Matter with Natural and Engineered Inorganic Colloids: A Review, *Environ. Sci. Technol.*, 2014, **48**(16), 8946–8962.

42 O. Oriekhova and S. Stoll, Heteroaggregation of nanoplastic particles in the presence of inorganic colloids and natural organic matter, *Environ. Sci.: Nano*, 2018, **5**(3), 792–799.

43 A. Clavier, A. Praetorius and S. Stoll, Determination of nanoparticle heteroaggregation attachment efficiencies and rates in presence of natural organic matter monomers. Monte Carlo modelling, *Sci. Total Environ.*, 2019, **650**, 530–540.

44 A. L. Dale, E. A. Casman, G. V. Lowry, J. R. Lead, E. Viparelli and M. Baalousha, Modeling Nanomaterial Environmental Fate in Aquatic Systems, *Environ. Sci. Technol.*, 2015, **49**(5), 2587–2593.

45 V. K. La Mer and T. W. Healy, Adsorption-flocculation reactions of macromolecules at the solid-water interface, *Rev. Pure Appl. Chem.*, 1963, **13**, 112–133.

46 J. Gregory, Rates of Flocculation of Latex Particles by Cationic Polymers, *J. Colloid Interface Sci.*, 1973, **42**(2), 448–456.

47 R. Hogg, Collision Efficiency Factors for Polymer Flocculation, *J. Colloid Interface Sci.*, 1984, **102**(1), 232–236.

48 W. L. Yu, F. Bouyer and M. Borkovec, Polystyrene sulfate latex particles in the presence of poly(vinylamine): Absolute aggregation rate constants and charging behavior, *J. Colloid Interface Sci.*, 2001, **241**(2), 392–399.

49 W. H. Pennock, M. L. Weber-Shirk and L. W. Lion, A Hydrodynamic and Surface Coverage Model Capable of Predicting Settled Effluent Turbidity Subsequent to Hydraulic Flocculation, *Environ. Eng. Sci.*, 2018, **35**(12), 1273–1285.

50 A. Moncho-Jorda, G. Odriozola, M. Tirado-Miranda, A. Schmitt and R. Hidalgo-Alvarez, Modeling the aggregation of partially covered particles: Theory and simulation, *Phys. Rev. E: Stat., Nonlinear, Soft Matter Phys.*, 2003, **68**(1), 011404.

51 N. K. Geitner, S. M. Marinakos, C. Guo, N. O'Brien and M. R. Wiesner, Nanoparticle Surface Affinity as a Predictor of Trophic Transfer, *Environ. Sci. Technol.*, 2016, **50**(13), 6663–6669.

52 A. A. Turner, N. M. K. Rogers, N. K. Geitner and M. R. Wiesner, Nanoparticle affinity for natural soils: a functional assay for determining particle attachment efficiency in complex systems, *Environ. Sci.: Nano*, 2020, **7**(6), 1719–1729.

53 N. K. Geitner, J. L. Cooper, A. Avellan, B. T. Castellon, B. G. Perrotta, N. Bossa, M. Simonin, S. M. Anderson, S. Inoue, M. F. Hochella, C. J. Richardson, E. S. Bernhardt, G. V. Lowry, P. L. Ferguson, C. W. Matson, R. S. King, J. M. Unrine, M. R. Wiesner and H. Hsu-Kim, Size-Based Differential Transport, Uptake, and Mass Distribution of Ceria (CeO<sub>2</sub>) Nanoparticles in Wetland Mesocosms, *Environ. Sci. Technol.*, 2018, **52**(17), 9768–9776.

54 N. K. Geitner, N. Bossa and M. R. Wiesner, Formulation and Validation of a Functional Assay-Driven Model of Nanoparticle Aquatic Transport, *Environ. Sci. Technol.*, 2019, **53**(6), 3104–3109.

55 G. Cornelis, Fate descriptors for engineered nanoparticles: the good, the bad, and the ugly, *Environ. Sci.: Nano*, 2015, **2**(1), 19–26.

56 P. A. Holden, J. L. Gardea-Torresdey, F. Klaessig, R. F. Turco, M. Mortimer, K. Hund-Rinke, E. A. C. Hubal, D. Avery, D. Barcelo, R. Behra, Y. Cohen, L. Deydier-Stephan, P. L. Ferguson, T. F. Fernandes, B. H. Harthorn, W. M. Henderson, R. A. Hoke, D. Hristozov, J. M. Johnston, A. B. Kane, L. Kapustka, A. A. Keller, H. S. Lenihan, W. Lovell, C. J. Murphy, R. M. Nisbet, E. J. Petersen, E. R. Salinas, M. Scheringer, M. Sharma, D. E. Speed, Y. Sultan, P. Westerhoff, J. C. White, M. R. Wiesner, E. M. Wong, B. S. Xing, M. S. Horan, H. A. Godwin and A. E. Nel, Considerations of Environmentally Relevant Test Conditions for Improved Evaluation of Ecological Hazards of Engineered Nanomaterials, *Environ. Sci. Technol.*, 2016, **50**(12), 6124–6145.

57 C. O. Hendren, G. V. Lowry, J. M. Unrine and M. R. Wiesner, A functional assay-based strategy for nanomaterial risk forecasting, *Sci. Total Environ.*, 2015, **536**, 1029–1037.

58 J. A. McKeague and M. G. Cline, Silica in Soils, *Adv. Agron.*, 1963, **15**, 339–396.

59 M. S. Croughan, J. F. Hamel and D. I. C. Wang, Hydrodynamic Effects on Animal-Cells Grown in Microcarrier Cultures, *Biotechnol. Bioeng.*, 1987, **29**(1), 130–141.

60 F. Gottschalk, T. Sonderer, R. W. Scholz and B. Nowack, Modeled Environmental Concentrations of Engineered Nanomaterials (TiO<sub>2</sub>, ZnO, Ag, CNT, Fullerenes) for Different Regions, *Environ. Sci. Technol.*, 2009, **43**(24), 9216–9222.

61 A. Franchi and C. R. O'Melia, Effects of natural organic matter and solution chemistry on the deposition and reentrainment of colloids in porous media, *Environ. Sci. Technol.*, 2003, **37**(6), 1122–1129.

62 K. Yang, D. H. Lin and B. S. Xing, Interactions of Humic Acid with Nanosized Inorganic Oxides, *Langmuir*, 2009, **25**(6), 3571–3576.

63 W. L. Li, P. Liao, T. Oldham, Y. Jiang, C. Pan, S. H. Yuan and J. D. Fortner, Real-time evaluation of natural organic matter deposition processes onto model environmental surfaces, *Water Res.*, 2018, **129**, 231–239.

64 Z. Adamczyk, *Particles at interfaces: interactions, deposition, structure*, Elsevier/Academic Press, Amsterdam; Boston, 1st edn, 2006, p. 743.

65 Z. Adamczyk and P. Belouschek, Localized Adsorption of Particles on Spherical and Cylindrical Interfaces, *J. Colloid Interface Sci.*, 1991, **146**(1), 123–136.

66 Z. Adamczyk and P. Weronski, Random sequential adsorption on partially covered surfaces, *J. Chem. Phys.*, 1998, **108**(23), 9851–9858.

67 N. C. Mueller and B. Nowack, Exposure modeling of engineered nanoparticles in the environment, *Environ. Sci. Technol.*, 2008, **42**(12), 4447–4453.

68 A. Praetorius, M. Scheringer and K. Hungerbuhler, Development of Environmental Fate Models for Engineered Nanoparticles-A Case Study of TiO<sub>2</sub> Nanoparticles in the Rhine River, *Environ. Sci. Technol.*, 2012, **46**(12), 6705–6713.